T020023-00-D
Signal Sensing in Advanced LIGO
Part I

Guido Mueller

17th March 2003

1 Introduction

The requirements for advanced LIGO depend on the inperfections and asymmetries in the interferometer and on the length sensing scheme. It is mandatory to specify the parameters used to calculate the sensitivities and requirements. The parameters for the mirrors are shown in table 1. The distances are shown in table 2.

The power in the carrier (without sidebands) in such an interferometer at the different locations is shown in table 3. The first configuration is identical to the one described in table 1. In the second configuration, we switched the two ETM mirrors. The difference in the intensity in the two arm cavities is in both cases about 1%. This is important for technical radiation pressure noise as the pressure in both arms scales with the intensity. The main difference between the two cases is the amount of carrier in the dark port (only TEM_{00}light, higher order modes will hopefully be suppressed by the output mode cleaner). The power levels are calculated without detuning the arm cavities.

2 The Signal

The transfer functions of the signal sidebands in such a configuration are shown in Fig. 1. There are three different frequency ranges. At low frequencies the amplitudes of the sidebands are equal and have the same $-90°$ phase shift . In the intermediate frequency range the upper sideband is much stronger than the lower sideband and its phase is shifted by $90°$. In the high frequency range both sidebands have again equal amplitudes but now opposite phases. These facts are important for the detection process and the optimum local oscillator in advanced LIGO.

2.1 DC-Sensing

The measured signal will be the power spectral density at the dark port. The local oscillator is the carrier itself. It is possible and useful to distinguish between two different

MIRROR	R	T	L
PR	0.93996	0.06	40ppm
BS	0.5	0.5	0
ITMY	0.994948	0.005025	27ppm
ETMY	0.999968	0	32ppm
ITMX	0.994982	0.004975	43ppm
ETMX	0.999952	0	48ppm
SR	0.92996	0.07	40ppm

Table 1: The parameters used in the various simulations are shown in here. Many noise sources and even the signal depend strongly on small differences in the reflectivities and transmissivities of the mirrors. We assumed losses of 40ppm for both recycling mirrors. This values is not critical. We also assumed average losses of 40ppm for both ETMs with a 20% difference. We also assumed average losses of 35ppm losses with a 20% difference for the ITMs. We also assume that the mirrors with more losses are all in the X-arm. This becomes important when we discuss the necessary differential detuning for DC-locking. These values were used to achieve a 1% intensity difference in the two arm cavities [1] at the appropriate power built up.

Length	[m]
l_{PR}	3.75
l_1	4.8
l_2	4.38
L_1	4000
L_2	4000
l_{SR}	3.737

Table 2: The various distances used in the simulation. $l_{P(S)R}$ is the distance between P(S)R-mirror and BS, $l_{1(2)}$ is the distance between ITMX(Y) and the BS. The detuning of the signal recycling mirror leads to an additional half trip phase shift of $\phi_{SR} = 3.4°$.

Loc	P (Conf. as above)	P (switched ETMX$\leftrightarrow$ETMY)
In	125 W	125 W
PR	2125 W	2127 W
ITMY	1007 W	1001.7 W
ITMX	994 W	1001.4 W
ETMY	819 kW	820 kW
ETMX	827 kW	828kW
SR	1.6 mW (Carrier) w/o detuning	.89 μW (Carrier) w/o detuning

Table 3: The power in the carrier at different locations in the interferometer. Note the 1% difference in the intensity in the two arms and the huge difference in the power at the dark port between these very similar designs.

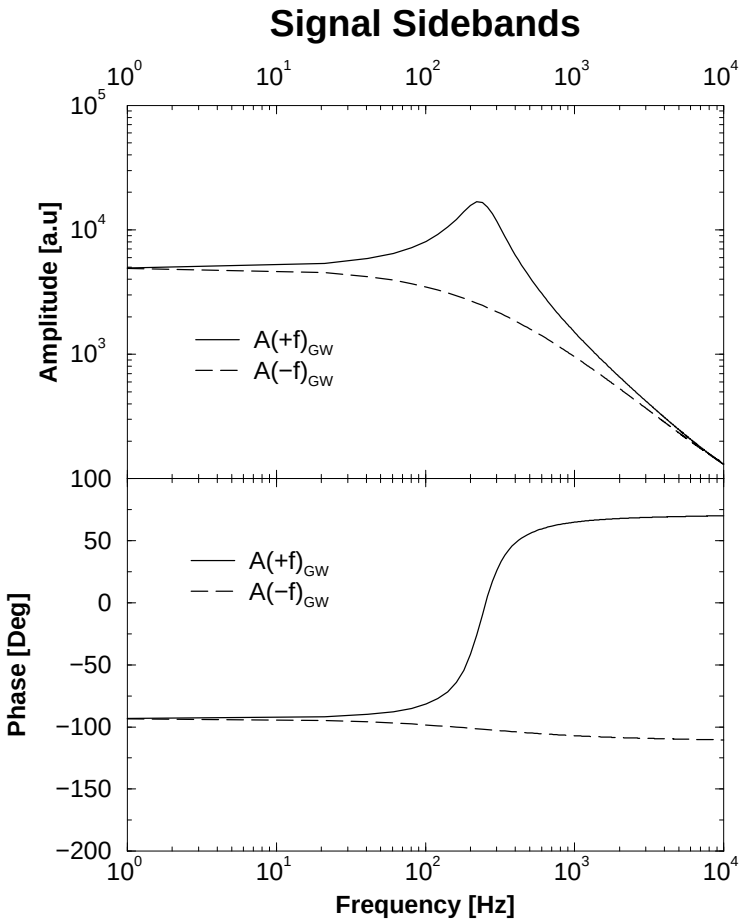

Figure 1: The transfer functions of the upper and lower signal sideband for the described configuration. These transfer function are not sensitive to minor changes in the losses in the different mirrors or if the arm cavities are detuned or not.

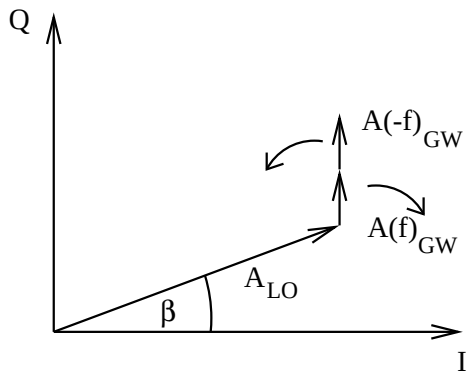

Figure 2: The signal sidebands $A(\pm f)_{GW}$ are rotating in this frame in opposite directions. Below the SR-resonance frequency they interfere constructively the moment they are parallel to the Q-component of the local oscillator A_{LO}. For this frequency range $\beta = \pm 90°$ would provide us with the best signal to (shot-) noise ratio.

quadrature components of the carrier. We define the inphase component I_{LO} of the carrier at the dark port if it is caused by a mismatch in the losses in the two arms. The intensity of this component is shown in table 3. The quadrature component Q_{LO} can be adjusted with a differential offset in one of the differential length degrees of freedom. The final local oscillator will be

$$A_{LO} = \sqrt{I_{LO}^2 + Q_{LO}^2}\, e^{i\beta} \qquad \tan\beta = \frac{I_{LO}}{Q_{LO}}$$

The sensitivity of the interferometer depends on the phase β of the local oscillator and is a function of the GW-frequencies.

2.1.1 Low Frequencies (< 70 Hz)

The signal can be constructed using phasor diagrams. For the low frequency region (see Fig. 2) the signal sidebands are rotating in opposite directions. They add up constructively when they are parallel to the Q-component and destructively the moment they are parallel to the I component. In other words for a local oscillator in the Q-quadrature, the sidebands create amplitude modulation. Beating with a local oscillator in the I-quadrature, the sidebands create phase modulation. Only amplitude modulation is visible on the photodetector. The optimum local oscillator phase is therefor $\beta = \pm 90°$. This would require a substantial differential detuning of the arm cavities.

2.1.2 Intermediate Frequencies (70 Hz > f > 700 Hz)

In the intermediate frequeny range the upper sideband builds up in the signal recycling cavity and the lower sideband is suppressed (see Fig. 3). The signal is essentially generated by the beat between the upper sideband and the local oscillator. The amplitude of

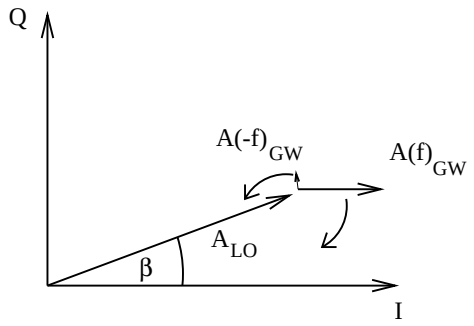

Figure 3: The upper sideband builds up and is responsible for the signal, while the lower sideband is more or less suppressed. The final photodiode signal measures the beat between the upper sideband and the LO. The amplitude of this signal does not depend on the phase of the local oscillator.

this beat is independent from the phase of the local oscillator. Any linear combination is fine.

2.1.3 High frequencies (f > 700 Hz)

Above the signal recycling resonance both signal sidebands become equal in amplitude again. The lower sideband is shifted from $-90°$ to $-110°$ in phase, while the upper sideband is shifted to 70°. In this case, the two sidebands interfere constructively when they are parallel to a local oscillator that is shifted by 20° relative to the inphase component I_{LO} of the carrier (see Fig. 4). The optimum local oscillator phase is $\beta = 20°$.

2.1.4 Summary

The sensitivities for the three cases $\beta = 0$, 20°, 90° are shown in Fig. 5. The first case has a very low sensitivity at low frequencies up to zero sensitivity at DC. But its sensitivity is better at high frequencies. The third case has a very good sensitivity at low frequencies and is not very good at high frequencies. At the resonance frequency, the difference between both quadratures vanish essentially. The optimum tuning for the high frequency range $\beta = 20°$ has also an increased sensitivity for low frequencies compared to the $\beta = 0°$ case. This can easily be understood when we look at the field at the dark port:

$$E_{dp} = (I + iQ) + E_+ e^{i2\pi ft} + E_- e^{-i2\pi ft}$$

where the E_+, E_- are the signal sidebands at frequency f.

At low frequencies, the sidebands are:

$$E_+(f \ll f_{res}) = -iE_s = E_-(f \ll f_{res})$$

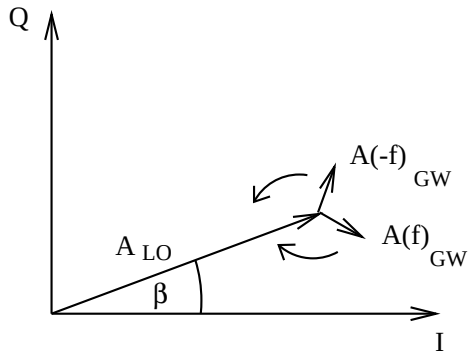

Figure 4: Above the SR-resonance the two sidebands have again roughly the same amplitude but the phase of the upper sideband has changed by about 180° relative to the lower sideband. The sidebands interfere in this case constructively when they are parallel to the inphase component I_{LO} of the carrier and destructively when they are parallel to the quadrature component Q_{LO} . The optimum local oscillator phase is now $\beta = 20°$.

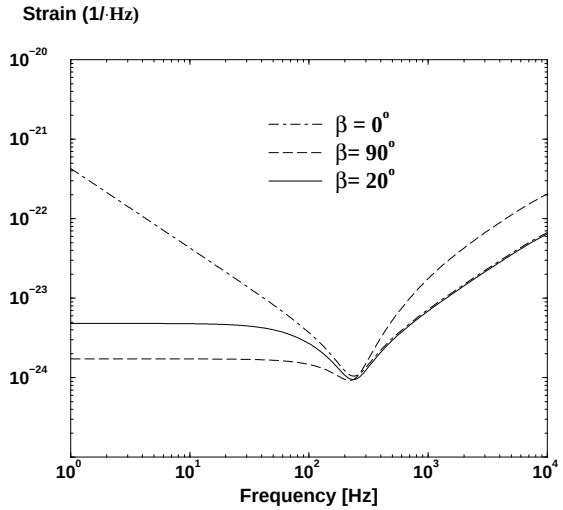

Figure 5: The strain sensitivity vs. shot noise for DC locking. $\beta = 0°$ assumes no detuning between the two arm. The carrier in the dark port is only caused by contrast defects because of different losses in the two arms. $\beta = 90°$ requires matched losses in the two arms and the carrier is caused by detuned arm cavities.

where E_s is the amplitude of the signal generated by a gravitational wave or any other differential displacement of the arm cavities. The power changes are in this case:

$$P_{dp}(f \ll f_{res}) = 2QE_s \cos 2\pi ft$$

In the high frequency range the signal sidebands can be written as:

$$E_+ = E_s e^{i\frac{70^\circ}{180^\circ}\pi} \qquad E_- = E_s e^{i\frac{-110^\circ}{180^\circ}\pi}$$

This turns into:

$$P_{dp}(f \gg f_{res}) = \Re\left\{(I+iQ)E_s e^{i\frac{70^\circ}{180^\circ}\pi}\left(e^{i2\pi ft} - e^{-i2\pi ft}\right)\right\}$$

$$= 2E_s\left(I\cos(20^\circ) + Q\sin(20^\circ)\right)\sin 2\pi ft$$

A local oscillator with $\beta = 20^\circ$ would give the maximum result. Compared to $\beta = 0^\circ$ we gain about 6% of the high frequency signal. But we also keep 34% of the low frequency signal. As the low frequency range is limited by radiation pressure noise and thermal noise and not by shot noise, it is most likely that this is the optimum tuning. It should not degrade the maximum possible signal by more than 10% at any frequency (most likely even less).

In the following we assume that we have the configuration described above with 1.6 mW carrier power at the dark port without detuning. The appropriate length tuning of the arm cavities to achieve $\beta = 20^\circ$ is 0.266 pm (one way, one arm. The total differential path length difference between the two arm cavities is then $4 * 0.266\,\mathrm{pm} \approx 1\,\mathrm{pm}$). This increases the total carrier power at the dark port to 1.86mW. Increased asymmetries in the arm cavity losses would result in an increase in the carrier power at the dark port without detuning and would require a larger differential detuning to achieve the correct β.

The resulting strain sensitivity including the other noise sources (fitted to the low frequency part of the sensitivity curve in [1]) is shown in Fig. 6.

The transfer function

$$P_{min}(f, \delta L_{min}) = T(f)\delta L_{min}(f) = T(f)Lh_{min}(f)$$

for differential length changes times the expected displacement sensitivity gives an upper limit for all power fluctuations in the signal not caused by gravitational waves. This needs to be divided by an additional factor of 10 to include the safety factor. This value increases with the square root of the intensity of the carrier (the local oscillator) at the dark port.

2.2 RF-Sensing

In an RF-sensing scheme the signal sidebands beat with two RF-sidebands at ± 179.7 MHz (for a 21 cm Schnupp asymmetry) off of the carrier. This beat is then demodulated with the RF-frequency using both quadratures. In principle the signal can be reconstructed by using the quadratic sum of both demodulated quadratures. As long as the

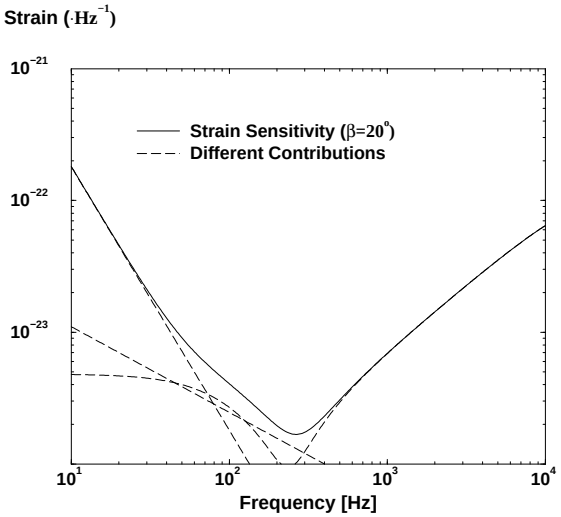

Figure 6: Strain Sensitivity for Advanced LIGO with $\beta = 20°$. Low frequency noise sources approximated from Fig 4 in [1], 125W curve.

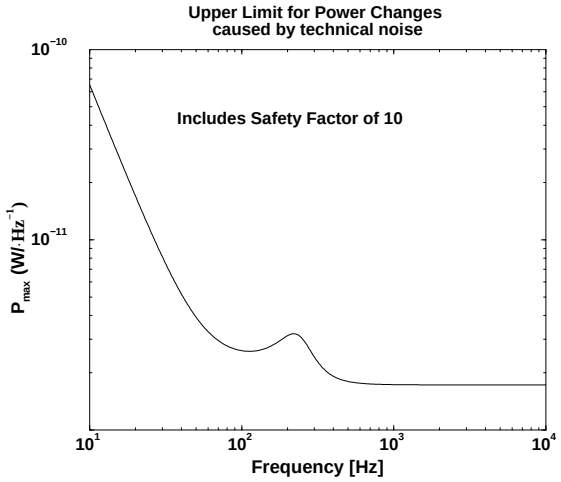

Figure 7: Changes in the power in the dark port field of this magnitude would be a tenth of the signal caused by gravitational waves at design sensitivity.

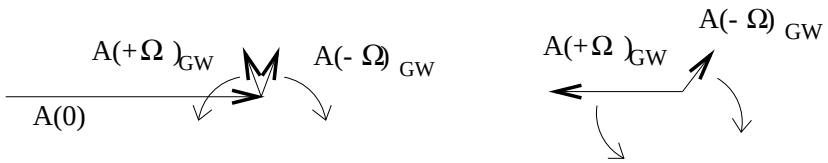

Figure 8: The left graph shows the phase modulated input field in a phasor diagram. The right graph the RF-sidebands at the dark port of Advanced LIGO. The carrier in the right graph is omitted for clarity. Its phase and amplitude depend on the asymmetries and the tuning. This is described in the DC-sensing part.

two demodulation phases are orthogonal this would be independent of the specific demodulation phases. But we will see that there is an optimum demodulation phase able to generate a signal that is very close to the optimum possible signal at all frequencies. The advantage is that we do not have to take the quadratic sum is not important. The advantage might be that specific technical noise contributions will show up mainly in the quadrature that is orthogonal to the optimum signal. This could reduce the requirements on technical noise by orders of magnitude.

The optical components and the distances between the mirrors are the same except that the distance between the SR mirror and the BS is reduced from 3.75 m to 3.74838 m. With this tuning the upper SB is now on resonance in the PR-SR cavity. It is assumed that we still have an output mode cleaner. This output mode cleaner is assumed to transmit the carrier, the signal sidebands, the RF-sidebands, and all noise sidebands in the fundamental spatial mode.

The amplitude of the input field can be written as:

$$E_{in} = \sqrt{125W}e^{i\omega t}e^{0.1i\cos\Omega t}$$

$$E_{in} = \sqrt{125W}\left(J_0(0.1) + iJ_1(0.1)\left(e^{i\Omega t} + e^{-i\Omega t}\right)\right)e^{i\omega t}$$

The two sidebands are both 90° out of phase with the carrier. The amplitudes (in units $\sqrt{W}$) are

$$\text{Carrier} = 11.12 \qquad \text{Both Sidebands} = 0.56$$

At the dark port the fields will have the following amplitudes and phases:

$$E_{dp} = |A_c|e^{i\Phi_c} + |A_+|e^{i\Phi_+} + |A_-|e^{i\Phi_-}$$

$$|A_c| = 0.032 \qquad \Phi_c = 177^\circ$$

$$|A_+| = 0.554 \qquad \Phi_+ = 180^\circ$$

$$|A_-| = 0.154 \qquad \Phi_- = 70^\circ$$

The amplitude of the upper sideband is 3.6 times larger than the amplitude of the lower sideband and about 13.9 times larger than the amplitude of the carrier. The phase of the upper sideband changes with about $6.3^\circ/\text{mm}$ change of the PRSR-cavity length. The phase of the lower sideband changes only with $0.53^\circ/\text{mm}$ (this is with respect

to a carrier that defines the same working point). A slightly off resonant SR-cavity will therefore change the phase relation between the two RF-sidebands, which in turn changes the optimum demodulation phase, the maximum possible signal, and probably the requirements on technical noise sources like laser amplitude or oscillator phase noise. Note, the amplitude of the leaking carrier is unimportant for the strength of the signal, but it might be very important for the requirements on the laser. It is the local oscillator for noise sidebands around the RF-sidebands.

The signal can be calculated from the transfer functions shown in Fig. 1. Each signal sideband beats with each RF-sideband and generates a signal at a frequency $\Omega \pm 2\pi f$. The field at the dark port has the following form:

$$E_{dp} = A_+ e^{i\Omega t} + A_- e^{-i\Omega t} + A(f) e^{i2\pi ft} + A(-f) e^{-i2\pi ft} + A_c$$

The intensity at frequencies $\Omega \pm 2\pi f$ has the general form:

$$\begin{aligned} I_{PD}(\Omega \pm 2\pi f) &= \Re\{A^*(f)A_+ + A^*(-f)A_-\}\cos((\Omega - 2\pi f)t) \\ &+ \Re\{A^*(-f)A_+ + A^*(f)A_-\}\cos((\Omega + 2\pi f)t) \\ &+ \Im\{A^*(-f)A_- - A^*(f)A_+\}\sin((\Omega - 2\pi f)t) \\ &+ \Im\{A^*(f)A_- - A^*(-f)A_+\}\sin((\Omega + 2\pi f)t) \end{aligned}$$

Demodulated with $\sin(\Omega t)$ and $\cos(\Omega t)$ these signals are:

$$\begin{aligned} I_{PD} * \cos\Omega t &= \Re\{(A^*(f) + A^*(-f))(A_+ + A_-)\}\cos 2\pi ft \quad (1) \\ &+ \Im\{(A^*(f) - A^*(-f))(A_+ + A_-)\}\sin 2\pi ft \quad (2) \end{aligned}$$

$$\begin{aligned} I_{PD} * \sin\Omega t &= \Re\{(A^*(f) - A^*(-f))(A_+ - A_-)\}\sin 2\pi ft \quad (3) \\ &- \Im\{(A^*(f) + A^*(-f))(A_+ - A_-)\}\cos 2\pi ft \quad (4) \end{aligned}$$

There are essentially four different parts. One part in each demodulated signal is proportional to the sum of the two signal sidebands $A(f) + A(-f)$ (proportional to $\cos 2\pi ft$) and one part in each demodulated signal is proportional to the difference $A(f) - A(-f)$ (proportional to $\sin 2\pi ft$). Each of these four parts has contributions from the upper and lower RF-sideband.

2.2.1 Low frequencies (f < 50 Hz)

One way to display the beats in a phasor type diagram is to add the two signal sidebands, beat the sum with each of the RF-sidebands, and finally add both contributions. In the low frequency range (see Fig. 1) the two signal sidebands have about the same amplitude and are both 90° out of phase with respect to the original carrier. In this picture they add up to one arrow that is parallel to the Q-axes or imaginary axes:

$$A(f) + A(-f) \approx i2|A(f)| \qquad f \ll f_{res}$$

The difference between the two sidebands is zero. Therefore the second part in the first demodulated signal 2 and the first part in the second demodulated signal 3 will vanish.

Upper RF-sideband

The remaining parts are:

$$I(A_+ \text{ only}) \sin\Omega t = -2|A(f)||A_+| \cos\Phi_+ \cos 2\pi f t$$

$$I(A_+ \text{ only}) \cos\Omega t = -2|A(f)||A_+| \sin\Phi_+ \cos 2\pi f t$$

In the design the upper RF-sideband is resonant in the PR-SR cavity. This implies that under the circumstances presented above (phase modulation with $\cos\Omega t$) it's amplitude A_+ is real ($\Phi_+ = 0, 180°$) and the second signal vanishes.

Lower RF-sideband

The lower sideband is not resonant in the PRSR cavity, but it is also not so far detuned that we could ignore it. Its amplitude is about a third of the amplitude of the upper sideband while its phase is 70°. It is mainly pointing into the imaginary direction, which implies that its main contribution to the signal will show up in the first part (1):

$$I(A_- \text{ only}) \cos\Omega t = 2|A(f)||A_-| \sin 70° \cos 2\pi f t \qquad \sin 70° = 0.94$$

A smaller signal will also show up in the forth part (4):

$$I(A_- \text{ only}) \sin\Omega t = 2|A(f)||A_-| \cos 70° \cos 2\pi f t \qquad \cos 70° = 0.34$$

Its size is about a tenth of the size of the upper RF-sideband contribution.

Optimum Demodulation Phase

The optimum demodulation phase can then be calculated as follows:

$$\phi_{demod} = \arctan \frac{A_+ \cos\Phi_+ - A_- \cos\Phi_-}{A_+ \sin\Phi_+ - A_- \sin\Phi_-} = 103.4° \qquad \text{for } \Theta_+ = 180°$$

Fig. 9 shows the situation in a phasor diagram. The two signal sidebands form an arrow that is changing its length along the imaginary axes. The projection onto the RF-sidebands is zero if they are perpendicular to the arrow. and reaches its maximum (minimum) value if they are parallel (antiparallel). The best demodulation phase for the beat between the upper sideband ($\Theta_+ = 180°$) and the signal sidebands is 90° out of phase compared to the phase modulation. The lower sideband has a phase of 70° relative to the positive real axis at the start time and its optimum demodulation phase would be 160° out of phase compared to the phase modulation. The overall optimized demodulation phase depends on the amplitudes of the two RF-sidebands and is in this case 103.4°.

2.2.2 Intermediate Frequencies (70 Hz < f < 700 Hz)

In the intermediate frequency range the upper signal sideband is much stronger than the lower signal sideband. Its phase also changes very quickly. The main contribution comes from the beat between the upper signal sideband and the upper RF-sideband.

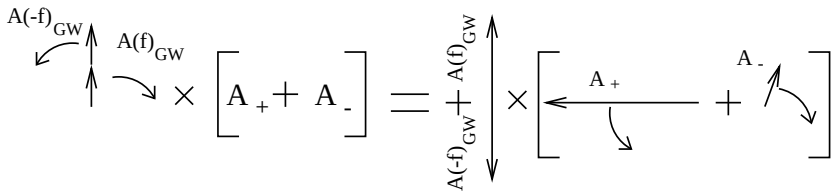

Figure 9: The beat between the low frequency signal sidebands $A(\pm f)_{GW}$ and the RF-sidebands is shown graphically in these phasor diagrams. See text for further explanations.

Upper RF-Sideband

Taking only into account the upper signal and the upper RF-sideband, the field can be written as:

$$E_{dp} = A_+ e^{i\Omega t} + A(f)e^{i2\pi ft} = \left(|A_+| + A(f)e^{i2\pi ft}e^{-i(\Omega t+\Phi_+)}\right)e^{i(\Omega t+\Phi_+)}$$

The intensity is:

$$I(A(f), A_+ \text{ only}) = |A_+|\left[\Re\left\{A(f)e^{i2\pi ft}\right\}\cos(\Omega t+\Phi_+) + \Im\left\{A(f)e^{i2\pi ft}\right\}\sin(\Omega t+\Phi_+)\right]$$

The amplitude of the signal is independent from the demodulation phase. Only the phase of the oscillating signal ($\propto \cos 2\pi ft, \propto \sin 2\pi ft$) does change.

A similar signal appears for the lower signal sideband:

$$E_{dp} = A_+ e^{i\Omega t} + A(-f)e^{-i2\pi ft} = \left(|A_+| + A(f)e^{-i2\pi ft}e^{-i(\Omega t+\Phi_+)}\right)e^{i(\Omega t+\Phi_+)}$$

The intensity is:

$$I(A(-f), A_+ \text{ only}) = |A_+|\left[\Re\left\{A(-f)e^{-i2\pi ft}\right\}\cos(\Omega t+\Phi_+) + \Im\left\{A(-f)e^{-i2\pi ft}\right\}\sin(\Omega t+\Phi_+)\right]$$

Again, the amplitude is independent from the demodulation phase.

However, both sidebands together will cause the signals to interfere constructively or destructively, depending on the actual phase between $A(f)$ and $A(-f)$. The optimum demodulation phase is therefor a function of the exact frequency for which we wish to optimize the interferometer. But as the amplitude of $A(-f)$ is about a factor 6 smaller around f_{res}, the difference between different demodulation phases is only about 16% (see Fig. 10).

Lower RF-sideband

A similar analysis can be made for the lower RF-sideband. The lower RF-sideband and the upper signal sideband in the field can be written as:

$$E_{dp} = |A_-|e^{i\Phi_-}e^{-i\Omega t} + A(f)e^{i2\pi ft} = \left(|A_-| + A(f)e^{i(2\pi ft+\Omega)t}e^{-i\Phi_-}\right)e^{-i\Omega t}e^{i\Phi_-}$$

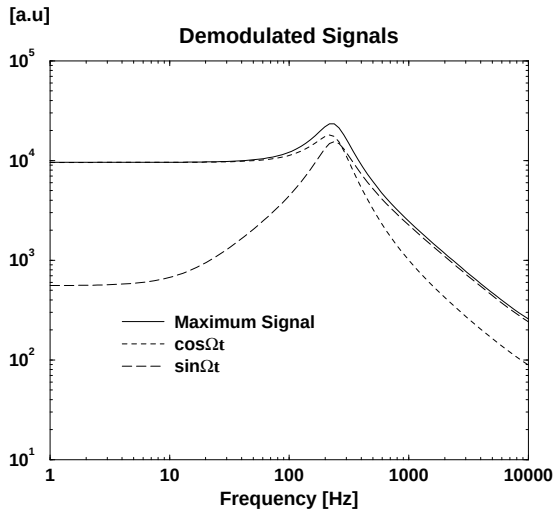

Figure 10: The signal for a single sideband scheme (or only upper RF-sideband in Advanced LIGO) for the inphase (dotted) and quadrature (dashed) demodulation. The solid line represents the optimum possible signal, the quadratic sum of the I and Q-signals.

and their beat in the intensity is

$$I(A(f),A_- \text{ only}) = |A_-| \left[\Re\left\{A(f)e^{i2\pi ft}\right\}\cos(\Omega t - \Phi_-) - \Im\left\{A(f)e^{i2\pi ft}\right\}\sin(\Omega t - \Phi_-)\right]$$

The lower signal sideband gives:

$$I(A(-f),A_- \text{ only}) = |A_-| \left[\Re\left\{A(-f)e^{-i2\pi ft}\right\}\cos(\Omega t - \Phi_-) - \Im\left\{A(-f)e^{-i2\pi ft}\right\}\sin(\Omega t - \Phi_-)\right]$$

The differences between the lower and upper RF-sideband signals are the strength, scaling with the amplitudes $|A_+|$, $|A_-|$, the shift in the demodulation phase Φ_+, Φ_-, and the -sign in the sin part.

Optimum Demodulation Phase

The total signal is the sum of all four contributions discussed above. Although the rms signal amplitude in each of the four signals is independent of the demodulation phase, the coherent sum of all four depends on it. The situation is different from the DC-case where the second contribution is so small compared to the first part that the difference between different LO-phases could be omitted. In the RF-case, the three smaller contributions combined can reduce (or increase) the beat between the upper signal and the upper RF-sideband significantly.

2.2.3 High Frequencies (f > 700 Hz)

The signal sidebands have again similar amplitudes but are shifted in phase. The difference between the sidebands is

$$A(f) - A(-f) = 2|A(f)|e^{i\frac{70}{180}\pi}$$

while the sum vanishes.

Upper RF-sideband

The upper RF-sideband will produce the following signals:

$$I = 2|A(f)||A_+|\sin 2\pi ft\,(\cos(\Phi_+ - 70°)\sin\Omega t + \sin(\Phi_+ - 70°)\cos\Omega t)$$

In other words, a demodulation with $\sin(\Omega t + \Phi_+ - 70°)$ would produce the full signal.

Lower RF-sideband

The lower RF-sideband produces essentially the same signal except that its amplitude is smaller because of the smaller amplitude of the RF-sideband and that the optimum demodulation phase is shifted by Φ_- instead of Φ_+:

$$I = 2|A(f)||A_-|\sin 2\pi ft\,(\sin(\Phi_- - 70°)\cos\Omega t - \cos(\Phi_- - 70°)\sin\Omega t)$$

The full signal can be obtained with a demodulation with $\sin(\Omega t - \Phi_- + 70°)$.

Optimum demodulation Phase

The optimum demodulation for the high frequency signals would be:

$$T \cdot \sin(\Omega t + \beta) \qquad \beta = atan\frac{|A_+|\sin(\Phi_+ - 70°) + |A_-|\sin(\Phi_- - 70°)}{|A_+|\cos(\Phi_+ - 70°) - |A_-|\cos(\Phi_- - 70°)} = -33.4°$$

for $\Phi_+ = 180°$.

2.2.4 Summary

The demodulated signals for various demodulation phases are shown in Fig. 11. The optimum demodulation phase is probably again the one with the best high frequency response ($\Phi_{demod} = -33.4°$). We will look into this when we analyse how different noise sidebands transmit through the interferometer. Under the assumption that we demodulate with $\Phi_{demod} = -33.4°$ the limits on power fluctuations in the demodulated light for technical noise sources can be obtained from Fig. 12.

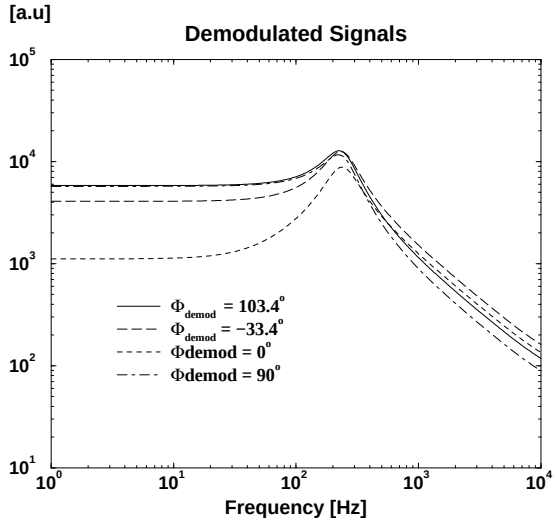

Figure 11: The demodulated signal for different demodulation phases. The first curve ($\Phi_{demod} = 103.4°$) has the best low frequency response, while the second curve ($\Phi_{demod} = -33.4°$) has the best high frequency response. The in-phase signal ($\Phi_{demod} = 0$) has a good high frequency response but is insensitive to low frequency signals and resonant signals. The quad-phase ($\Phi_{demod} = 90°$) has the worst high frequency response of these four shown signals.

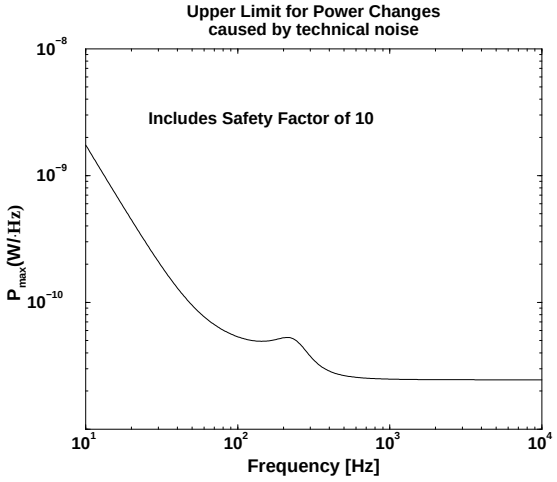

Figure 12: The minimum power in the demodulated signal allowed for technical noise. For a different demodulation phase (not optimized for high frequency GW), the requirements at low frequencies will be slightly relaxed, while the allowed signal at high frequencies will be smaller.

2.3 Summary

We calculated the optimum carrier for DC-sensing and the optimum demodulation phase for RF-sensing. In both cases the solution depends on the target frequency. For the solutions presented here, We assume that we optimize the detection process for the high frequency response. This optimization can only be made with respect to shot noise and not to displacement noise (RPN, thermal noise). Because the low frequency region is limited by displacement noise, the high frequency optimization should be the best we can ask for (?).

The optimum carrier for DC-locking is then very straightforward and it should be possible to tune the interferometer to get fairly close to that point. The optimum RF-demodulation phase depends strongly on the phase difference and amplitude difference of the two RF-sidebands. The phase of the resonant (upper) sideband is particularly sensitive to the length of the PRSR-cavity. Still, an optimization for the given length should be possible during commissioning of the detector. In both cases, the signal changes with the cosine of the difference from the optimum demodulation phase. This dependency is weak and it will not be very difficult to get so close to that point that the difference in signal strength is neglectable.

More important than the optimum demodulation phase in both schemes is the question: Can we reduce the sensitivity of the detector to technical noise contributions like laser amplitude noise or oscillator phase noise by tuning the demodulation phase around its optimum point? This will be investigated in the future.

3 Finesse-Code

The Finesse Code used to calulate the tranfer functions for DC-sensing. The modulators are still included without specific reason.

```
m pr 0.93996 0.06 0.0 mp_1 mp_2
s lp 3.75 mp_2 bs1_0
bs bs1 .5 .5 45 0 bs1_0 bs1_1 bs1_2 bs1_3
s l1 4.8 bs1_1 mi1_1
s l2 4.38 bs1_2 mi2_1
m itm1 0.99494 8 0.005025 -0.000
mi1_1 mi1_2 s lcav_1 4000 mi1_2 me1_1
m etm1 0.999968 0 -0.00009 me1_1 me1_2
m itm2 0.994982 0.004975 0.000 mi2_1 mi2_2
s lcav_2 4000 mi2_2 me2_1
m etm2 0.999952 0 0.00009 me2_1 me2_2
s ls 3.737 bs1_3 ms_1
m sr 0.92996 0.07 93.44 ms_1 ms_2
l i1 125 0 n1
mod eo1 9M 0.000000001 2 pm n1 n2
mod eo2 179716394 0.0000000000001 2 pm n2 mp_1
fsig sig1 etm1 100 0
fsig sig1 etm2 100 180
```

```
%ad out1 100 ms_2 %upper Signal SB amplitude
%ad out2 -100 ms_2 %lower Signal SB amplitude
%pdS1 out1 100 max ms_2 %shot noise limited detection
pd1 out1 00 max ms_2 %signal
xaxis sig1 f log 1 10000 501
xparam out1 f 1 0
yaxis log abs
scale meter
gnuterm x11
```

References

[1] *Advanced LIGO Systems Design,* LSC ed. Peter Fritschel LIGO-T010075-00-D